

Multiwavelength studies of WR 21a and its surroundings

Paula Benaglia^{1,2,*}, Gustavo E. Romero^{1,2,*}, Bärbel Koribalski³, A. M. T. Pollock⁴

¹ Instituto Argentino de Radioastronomía, C.C.5, (1894) Villa Elisa, Buenos Aires, Argentina

² Facultad de Cs. Astronómicas y Geofísicas, UNLP, Paseo del Bosque S/N, (1900) La Plata, Argentina

³ Australia Telescope National Facility, CSIRO, PO Box 76, Epping, NSW 1710, Australia

⁴ XMM-Newton Science Operations Centre, European Space Astronomy Centre, Apartado 50727, 28080 Madrid, Spain

June 19, 2018

Abstract. We present results of high-resolution radio continuum observations towards the binary star WR 21a (Wack 2134) obtained with the Australia Telescope Compact Array (ATCA**) at 4.8 and 8.64 GHz. We detected the system at 4.8 GHz (6 cm) with a flux density of 0.25 ± 0.06 mJy and set an upper limit of 0.3 mJy at 8.64 GHz (3 cm). The derived spectral index of $\alpha < 0.3$ ($S_\nu \propto \nu^\alpha$) suggests the presence of non-thermal emission, probably originating in a colliding-wind region. A second, unrelated radio source was detected $\sim 10''$ north of WR 21a at $(\text{RA}, \text{Dec})_{\text{J}2000} = (10^{\text{h}}25^{\text{m}}56^{\text{s}}.49, -57^{\circ}48'34.4'')$, with flux densities of 0.36 and 0.55 mJy at 4.8 and 8.64 GHz, respectively, resulting in $\alpha = 0.72$. H_I observations in the area are dominated by absorption against the prominent H_{II} region RCW 49. Analysis of a complete set of archived X-ray observations of WR 21a confirms its strong variability but throws into doubt previous suggestions by Reig (1999) of a period of years for the system. Finally, we comment on the association with the nearby EGRET source 3EG J1027-5817.

Key words. stars: early-type — stars: individual: WR 21a — stars: mass loss — stars: winds, outflows — radio continuum: stars — ISM: bubbles — gamma-rays: observations

1. Introduction

Massive O and Wolf-Rayet (WR) stars lose large amounts of mass through dense, energetic winds. These winds can interact with the surrounding interstellar medium (ISM) to create cavities in the H_I distribution (e.g. Benaglia & Cappa 1999) or produce strong shock fronts that, in principle, can accelerate charged particles up to relativistic energies (e.g. Völk & Forman 1982). In fact, non-thermal radio emission has been detected in a number of early-type stars, indicating the presence of populations of locally accelerated electrons (e.g. Chapman et al. 1999, Benaglia et al. 2001b, Benaglia & Koribalski 2004).

Particle acceleration mediated by strong shocks could be taking place in a number of different regions of a massive stellar system such as the outer boundary of the interaction between the wind and the ISM (e.g. Cassé & Paul 1980), the base of the wind, where line-driven instabilities are thought to drive strong shocks (e.g. White 1985), or, in

massive binary systems, the colliding-wind region (CWR, e.g. Eichler & Usov 1993). In addition to the expected non-thermal radio emission from relativistic electrons, high-energy radiation could be produced through, for example, inverse-Compton scattering of UV stellar photons or hadronic interactions from shock-accelerated ions and ambient material (e.g. Pollock 1987, White & Chen 1992, Romero et al. 1999, Benaglia et al. 2001a, Mücke & Pohl 2002, Benaglia & Romero 2003).

Only a small number of non-thermal radio WR binaries have been identified so far (see for instance Dougherty et al. 2003) and, even then, the connection between the radio and X-ray properties of these systems is far from clear. The archetype system WR 140 is bright in both regimes with a well-defined radio light curve that shares the 7.94-year period of the optical radial-velocity orbit. The X-ray light curve is not so well determined but shows strong variability consistent with the same period. WR 140, however, is the exception. The radio brightest star, WR 146, is a relatively faint X-ray source whereas WR 147 seems to be intermediate in both regimes. Sharing some characteristics with these systems, the star WR 21a [$(\alpha, \delta)_{\text{J}2000} = 10^{\text{h}}25^{\text{m}}56^{\text{s}}.49, -57^{\circ}48'44.4''$, $(l, b) = 284^{\circ}.52, -0^{\circ}.24$], is particularly interesting for various reasons. In the past, it coincided within the fairly large positional uncertain-

Send offprint requests to: P. Benaglia

e-mail: pbenaglia@fcaglp.unlp.edu.ar

* Member of Carrera del Investigador, CONICET

** The Australia Telescope is funded by the Commonwealth of Australia for operation as a National Facility managed by CSIRO.

ties with the COS B source 2CG 284-00 (Goldwurm et al. 1987). More recently, the unidentified EGRET gamma-ray source 3EG J1027-5817 was detected southwest of WR 21a (Hartman et al. 1999), being the star 30 arcmins apart from the center of the gamma-ray source. The 95% probability radius of the EGRET source is about 0.3°.

Caraveo et al. (1989) established that WR 21a is associated with the X-ray source 1E 1024.0-5732, and reported X-ray pulses. Its X-ray emission could be explained if the star is part of a binary system with either a compact companion forming a high-mass X-ray binary (Caraveo et al. 1989) or another massive, early-type star, with a CWR (Reig 1999). According to its stellar spectrum, it was early classified as an O5 star (Caraveo et al. 1989), and as a likely binary (WN5-6+O3f), at a maximum distance of 3 kpc (Reig 1999).

With the current investigation we aim at determining the radio properties of the star and its surroundings. Specifically, using interferometric observations at 3 and 6 cm, we looked for non-thermal radiation that might be interpreted as evidence for sites where electrons are being accelerated in colliding winds or terminal shocks. By means of low-resolution 21cm-line observations, we have also studied the distribution of neutral hydrogen around the star. The detection of non-thermal emission coincident with the stellar position would help in the identification of the system components. Analysis of all available X-ray data of WR 21a reveals a variability history that sheds fresh light on the nature of the binary. Finally, we discuss the possibility of a physical link between the stellar system and the nearby EGRET source, which can help to unveil the nature of the latter.

The contents of the paper are as follows: Section 2 reviews the main sources detected in this region of the sky that are relevant for the present study. Section 3 describes the observations carried out and the data reduction; Section 4 outlines the new observational results, whereas Section 5 presents the corresponding analysis. In Section 6 we discuss the X-ray data. Section 7 contains a comment on the possibility of a physical association between the star and the EGRET source 3EG J1027-5817. Section 8 closes with the summary.

2. WR 21a and its surroundings

The region of the Galactic plane towards $(l, b) = (284^\circ, 0^\circ)$ has been widely observed, from radio to gamma rays. The optical images of Rodgers et al. (1960) revealed various H II complexes, of which RCW 49 is the most prominent. The COS B satellite discovered the unidentified γ -ray source 2CG 284-00 (Bignami & Hermsen 1983, Caraveo 1983). The zone was then investigated by means of Einstein X-ray measurements in which were detected emission from RCW 49 and a point source named 1E 1024.0-5732 (Goldwurm et al. 1987). The point source was tentatively linked to WR 21a (Hertz & Grindlay 1984), an emission-line star with $m_V = 12.8$ (Wackerling 1969), also called Th35-42 and Wack 2134.

Caraveo et al. (1989) gathered enough evidence definitely to associate the X-ray source with the star. They took optical stellar spectra with the 3.6-m telescope at La Silla, classified the star as O5, set an upper limit for the stellar distance of 3 kpc, and studied the Einstein X-ray emission, reporting an X-ray periodicity of ~ 60 ms. They explained the X-ray behaviour as a binary with a compact companion, likely an accreting neutron star (NS). Dieters et al. (1990) looked for optical pulsations with the Tasmania 1-m telescope. They set an upper limit around 19.7 mag for any optical pulsation.

Mereghetti et al. (1994) observed the region with the ROSAT PSPC instrument, finding no pulsations, and obtained a further spectrum with the CTIO 1.6m telescope, revising the spectral classification to WN6. Based on the small equivalent widths of the emission lines, they suggested that the object could be a binary with an O star, rather than a compact companion, in which case the X-rays could come from colliding winds, in common with other Wolf-Rayet binary systems.

In 1999, Reig presented RXTE data and a new spectrum taken with the 1.9m telescope at SAAO. He stated that the lack of pulsations and the relatively soft and low X-ray emission seem to exclude the presence of a NS as responsible for the observed X-rays. Claiming that the spectrum shows features of both WR and O stars, he suggested that the system is formed by a WN6 and a possibly supergiant O3 companion, favoring the hypothesis of the colliding-wind binary (CWB). Roberts et al. (2001) observed the region towards WR 21a with ASCA, and interpreted the hard X-ray emission detected as produced by shocks from colliding winds in the stellar system. Very recently, Niemela et al.'s (2005) optical radial measurements have finally confirmed that the system is formed by two massive stars.

The distance d to WR 21a is not well established. We shall adopt $d = 3$ kpc throughout this paper, a value that seems to be consistent, as we will see, with all current observations.

Table 1 lists the adopted parameters that make up the Wack 2134/WR 21a binary system. Very few of the properties have so far been measured, so we have to assume parameters from similar stars or theoretical predictions. The stellar luminosity, effective temperature, and stellar mass of the WR component were estimated as an average of the same variables given by Hamann et al. (1995) for WN6 stars. The WR mean molecular weight of the ions μ was assumed the same as in Leitherer et al. (1997) for a WN6 star. The WR wind terminal velocity is taken as a mean value between data listed by Hamann et al. (1995) and by Prinja et al. (1990) for WN6 stars. The WR predicted mass loss rate (\dot{M}) is taken as the lowest value tabulated for WN6 stars by Nugis & Lamers (2000), in their compilation of observable M , and it can be considered a lower limit. The O3 (I) mass was taken as the spectroscopic mass from the tables of Vacca et al. (1996), and its terminal velocity from the averaged values listed by Prinja et al. (1990). We assumed $\mu = 1.5$ for the O

Table 1. Adopted stellar parameters for the binary system WR 21a

Variable	WR	OB	unit
Spectral Class.	WN6 ^(a)	O3 (I)f ^(b)	
$\log(L/L_\odot)$	5.2 ^(c)	6.274 ^(d)	
T_{eff}	45000 ^(c)	50680 ^(d)	K
M_*	12 ^(c)	65 ^(d)	M_\odot
μ	4 ^(c)	1.5 ^(c)	
v_∞	2000 ^(c)	3150 ^(c)	km s^{-1}
\dot{M} expected	3.0×10^{-5} ^(c)	1.4×10^{-5} ^(c)	$M_\odot \text{ yr}^{-1}$
distance d	3 ^(c)	3 ^(c)	kpc

(a) van der Hucht 2001; (b) Reig 1999; (c) see text;

(d) Vacca et al. 1996

star because of its evolved stage. A predicted mass loss rate was estimated using the recipe derived by Vink et al. (2000) (astro.ic.ac.uk/~jvink/). The expected (WR+Of) mass-loss rate would imply a 6-cm flux density of 0.24 mJy at 3 kpc, if thermal emission from ionized winds in both stars is assumed.

Close to WR 21a there are two interesting sources: the H II region RCW 49, and the gamma-ray source 3EG J1027–5817. They are discussed below.

2.1. The H II region RCW 49

RCW 49 is a southern H II region, located at $(l, b) = (284.3^\circ, -0.3^\circ)$, and extended over an area of $\sim 90' \times 70'$. Values for its distance range between 2.3 and 7.9 kpc (Manchester et al. 1970, Moffat et al. 1991, Brand & Blitz 1993, etc). H I spectra towards RCW 49 taken by Goss et al. (1972) show prominent H I absorption from about -20 to $+5 \text{ km s}^{-1}$ (see also Figs. 2 and 3). Whiteoak & Uchida (1997) have imaged RCW 49 at radio continuum with MOST at 0.843 GHz, and the central region using ATCA at 1.38 and 2.38 GHz, attaining an angular resolution of 7 arcsec. They found two shells, and ascribe the formation of the northern one to the Westerlund 2 cluster containing the binary star WR 20a, and the southern one to the star WR 20b (see their Fig. 2d). Recent infrared images of RCW 49 obtained with the Spitzer Space Telescope (Churchwell et al. 2004) show the intricate filamentary structure of the nebula in the inner 5 arcmin shaped by stellar winds and radiation.

2.2. The gamma-ray source 3EG J1027–5817

After the analysis of the EGRET data, Hartman et al. (1999) were the first to point at the proximity between the gamma-ray source 3EG J1027–5817 and the X-ray source 1E 1024.0–5732, associated with WR 21a (see Figure 3). The averaged measured flux at $E > 100$ MeV is $65.9 \pm 0.70 \times 10^{-8}$ photons $\text{cm}^{-2} \text{ s}^{-1}$. The source is constant within errors on timescales of months (variability index $I = 1.6$, see Torres et al. 2001) and with a photon spectral index $\Gamma = 1.94 \pm 0.09$ ($dN/dE \propto E^{-\Gamma}$). The more

recent variability analysis by Nolan et al. (2003), who calculated a likelihood function for the flux of each source in each observation, also suggests that this source is not variable on short, monthly timescales.

3. Observations and data reduction

In order to search for non-thermal radio emission in the direction of WR 21a we have carried out interferometric radio continuum observations at high angular resolution ($1'' - 2''$). These were complemented with single-dish H I-line observations to map the distribution of neutral material in the neighbourhood and study its kinematic behaviour.

3.1. Radio continuum observations

Radio continuum data were obtained in September 2001 with the Australia Telescope Compact Array in the 6D array, observing simultaneously at 3 and 6 cm, or 8.64 and 4.8 GHz, respectively. The total bandwidth used was 128 MHz. The primary calibrator was PKS 1934-638, with flux densities of 5.83 and 2.84 Jy, at 4.8 and 8.64 GHz. WR 21a was tracked 12 h –full synthesis– to gain maximum *uv* coverage, interleaving with observations of the phase calibrator 1039–47. The theoretical r.m.s. noise after ~ 9 h on source is 0.03 mJy at both frequencies, taking all baselines into account.

The data were reduced and analyzed with MIRIAD routines. The images built using “robust” weighting showed the best signal to noise ratio, and minimized sidelobes. The diffuse emission from extended sources was removed by taking out the visibilities corresponding to the shortest baselines. The resulting beams were $0.83'' \times 0.70''$ at 3 cm, and $1.73'' \times 1.49''$ at 6 cm. The r.m.s. noise of the final maps is $0.1 \text{ mJy beam}^{-1}$ at 3 cm and $0.06 \text{ mJy beam}^{-1}$ at 6 cm. The difference between the theoretical and the observed r.m.s. noise is mainly due to flagging of bad data –specially at 3 cm– as well as short baselines contributing with confusing emission from extended sources both in and outside the main beam.

The observations were set to optimize the detection of point-like features. Maps at two frequencies would allow the determination of spectral indices.

3.2. H I-line observations

The 21cm-line data were obtained with a 30m-single dish radiotelescope at the Instituto Argentino de Radioastronomía (IAR, Villa Elisa, Argentina) in June 2000. The observations were done in total power mode, covering a total field of $5^\circ \times 5^\circ$, in Galactic coordinates with a cell size of $15' \times 15'$. The HPBW at 1420 MHz is $30'$. The receiver’s system temperature was ≈ 35 K. The velocity coverage was $(-450, +450) \text{ km s}^{-1}$; the 1008 channel autocorrelator allows a maximum velocity resolution of 1.05 km s^{-1} . The r.m.s. noise of the brightness-temperature (T_B) of a single spectral point is ~ 0.1 K.

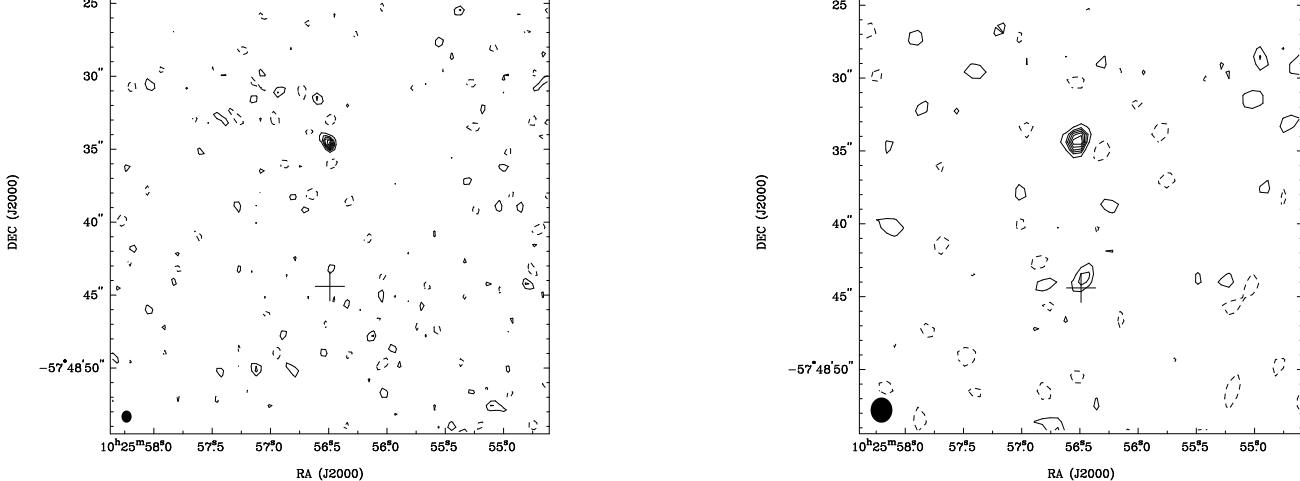


Fig. 1. *Left panel:* ATCA-3cm radio continuum image towards WR 21a. The optical position of the star is marked with a cross. The contour levels are $-0.20, 0.20 (2\sigma), 0.30, 0.35, 0.40, 0.45, 0.50$, and $0.55 \text{ mJy beam}^{-1}$. The synthesized beam ($0.83'' \times 0.70''$) is displayed at the bottom left corner. *Right panel:* ATCA-6cm radio continuum image towards WR 21a. The contour levels are $-0.12, 0.12 (2\sigma), 0.18, 0.24, 0.30$, and $0.33 \text{ mJy beam}^{-1}$. The synthesized beam ($1.73'' \times 1.49''$) is displayed at the bottom left corner.

The T_B scale was calibrated with the standard region S9 (Morras & Cappa 1995). A series of (l, b) - T_B maps were built every 1.05 km s^{-1} to proceed with the analytical stage.

4. Results

4.1. ATCA radio continuum data

The ATCA images at 3 and 6 cm are shown in Figure 1. A point source positionally coincident with WR 21a is visible at 6 cm, at $S/N > 4$. A flux density $S_{6\text{cm}} = 0.25 \text{ mJy}$ was derived using IMFIT after a gaussian fit (see Table 2). The r.m.s. noise in the 3 cm image is $0.1 \text{ mJy beam}^{-1}$. No radio source is detected at the stellar position above 3 r.m.s.. This non-detection imposes an upper limit for the spectral index of $\alpha < 0.3$ ($S \propto \nu^\alpha$). The deviation from purely thermal emission, characterized by $\alpha = 0.6 - 0.8$, indicates the presence of a non-thermal contribution.

In a similar way as in Benaglia & Koribalski (2004), we derive a mass loss rate of WR 21a, from the flux density at 6 cm. In a first approximation, the mean number of electrons per ion (γ), and the rms ionic charge (Z) were taken equal to unity. The gas temperature is computed from the stellar effective temperature (see Table 1) as $0.4 T_{\text{eff}}$. The Gaunt factor results in 5.6. At the adopted distance of 3 kpc, this would imply a radio-derived mass loss rate for the WR star of $\dot{M} = f \times 4.8 \times 10^{-5} \text{ M}_\odot \text{ yr}^{-1}$, where f is the fraction of thermal to total radio emission. From the relation between the flux density values measured with ATCA at 3 and 6 cm we know that at 6 cm there is a non-thermal contribution to the emission. Thus, in deriving a mass loss rate from the flux density at 6 cm, the result with $f = 1$ is an upper limit.

A second source, called S2, is detected $10''$ away from WR 21a, at both frequencies. The measured fluxes are

0.55 mJy at 3 cm, and 0.36 mJy at 6 cm. The corresponding spectral index of $\alpha_{S2} = +0.72$ points to an ultracompact H II region or the thermal wind of another, as yet unidentified, early-type star on the field of WR 21a. Table 2 lists the position and flux density of the two sources detected.

4.2. Large-scale H I-line data

Studies of neutral hydrogen were performed to look for evidences of gas features such as shells, filaments, bubbles, etc., that could be physically related to the object under the present study. The H I gas kinematics in the line-of-sight to a Galactic source can be used to constrain its distance (*e.g.* Koribalski et al. 1995) using the Galactic rotation curve (*e.g.* Fich et al. 1989) and the Galactic velocity field (Brand & Blitz 1993). Here we searched for the signatures of an interstellar H I bubble, created by the action of the stellar winds of WR 21a. Because of the large angular size of the IAR telescope beam (HPBW = 30 arcmin; see Figs. 2 and 3) and the proximity of WR 21a to the extended H II region RCW 49, which has a total radio continuum flux of $\sim 210 \text{ Jy}$ at 843 MHz (Whiteoak & Uchida 1997), H I spectra in this direction are completely dominated by H I absorption against RCW 49 (Goss et al. 1972; McClure-Griffiths et al. 2001). We also investigated the high-resolution (130 arcsec) H I data cubes from the Southern Galactic Plane Survey (SGPS; McClure-Griffiths et al. 2001) in the region of RCW 49 and WR 21a. Unfortunately, the region around RCW 49, including the H I line emission at the position of WR 21a, suffers from artifacts caused by the strong radio continuum emission from RCW49 and potential H I structures associated with WR 21a cannot be distinguished.

Table 2. Radio continuum results

Object	$S_{3\text{cm}}$ (mJy)	$S_{6\text{cm}}$ (mJy)	RA,Dec (J2000) (hms, dms)	α
WR 21a	< 0.3	0.25 ± 0.06	10:25:56.49 –57:48:43.3	< 0.3
S2	0.55 ± 0.10	0.36 ± 0.06	10:25:56.49 –57:48:34.4	0.72

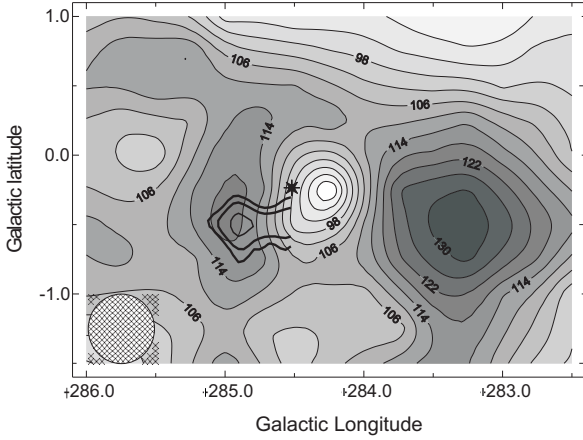


Fig. 3. Neutral-hydrogen column density integrated over velocities from -21 to -14 km s^{-1} . The contour levels indicate H I brightness temperatures in steps of 4 Kelvin. The IAR telescope beam is displayed in the bottom left corner. The position of WR 21a is marked with a black star, and the black contours represent the 99, 95 and 50% probability contours for the location of the gamma-ray source 3EG J1027-5817.

Figure 2 displays the H I brightness temperature maps each 4 km s^{-1} built from the IAR data.

If we were able to see an H I bubble around WR 21a, its size would give us some information about the energetics of the stellar wind and its velocity would give us an estimate of its kinematic distance using the Galactic rotation curve and velocity field. These issues are explored in the following section.

5. Analysis of the line features

The derivation of gas kinematic distances is difficult for this particular region of the Galactic plane. The line of sight goes tangential to the Carina arm at this Galactic longitude, and velocity crowding becomes very important. Brand & Blitz (1993) showed that the measured velocities deviate strongly from Galactic rotation: gas in the velocity range from -20 to -10 km s^{-1} can be located at distances between 2 and 6 kpc for $l \sim 285^\circ$, where both WR 21a and RCW 49 are likely to be located.

By means of CO observations, Grabelsky et al. (1987) studied molecular gas associated with the Carina arm. They interpreted the velocity-longitude behaviour of the gas in terms of material at different heliocentric distances

(see their Fig. 5), separating local clouds from Carina arm gas. According to their results it is possible to determine that toward $l \sim 284^\circ$ gas showing velocities around $\sim -15 \text{ km s}^{-1}$ belongs to the Carina arm and is located at about 3 kpc, i.e., the distance of WR 21a. In Fig. 2 it can be appreciated that the gas distribution changes at about $v \sim -14$ to -12 km s^{-1} . We are going to focus on gas with $\Delta v = -20$ to -12 km s^{-1} because, according to the CO results, its kinematical distance is compatible with that of the target star. The H I column density at the mentioned velocity interval is presented in Fig. 3. From the plot of Grabelsky et al. (1987), CO gas with velocities between -20 and -10 km s^{-1} is located between 2 and ~ 3.5 kpc. This fact helps to constrain an approximate error in the H I distance of ≤ 1 kpc. At larger velocities, Grabelsky et al. claimed that gas related to RCW 49 shows velocities of -5 km s^{-1} , and placed it at 4 kpc. A distance of ~ 5 kpc can be derived, for Carina gas with velocities near 0 km s^{-1} . If the H I follows the motions proposed by Grabelsky et al., it is reasonable to suggest that gas with a velocity of -14 km s^{-1} lies at 3 kpc.

Figure 3 shows the presence of gas at a distance compatible with that of the stellar system. Due to the strong continuum source RCW 49, part of the H I gas is not emitting but absorbing. At a distance of 3 kpc, the visible neutral gas coincident with the position of the EGRET source would sum up about $1500 M_\odot$, which can be considered as a lower limit for the masses of clouds at the distance we are interested on.

By means of Antenna I at IAR (HPBW = 12.4°) we also measured the H125 α (3326.9880 MHz) radio recombination line (RRL) towards $(l, b) = (284.32^\circ, -0.34^\circ)$. Since RRLs are typically produced by H II regions, the detected emission (see Fig. 4) is likely to be mostly from RCW 49. We measure a center velocity of $v = +0.6 \pm 1.4 \text{ km s}^{-1}$, similar to those found at other RRLs in RCW 49 (e.g. Caswell & Haynes 1987).

The kinetic energy needed to form a typical bubble around WR 21a can be computed as $E_k = 0.5M_{\text{sh}}v_{\text{exp}}^2 = 10^{49} \text{ erg}$ if we assume a shell mass of $M_{\text{sh}} = 10000 M_\odot$ and an expansion velocity of $v_{\text{exp}} = 10 \text{ km s}^{-1}$, which are typical parameters of neutral shells detected around massive O stars (Cappa & Benaglia 1998, Benaglia & Cappa 1999).

The stellar wind luminosity can be expressed as $L_w = 0.5\dot{M}v_\infty^2$. Using the values of \dot{M} and v_∞ given in Table 1, we find $L_{w,\text{WR}} = 3.8 \times 10^{37} \text{ erg s}^{-1}$, and $L_{w,\text{O}} = 4.4 \times 10^{37} \text{ erg s}^{-1}$.

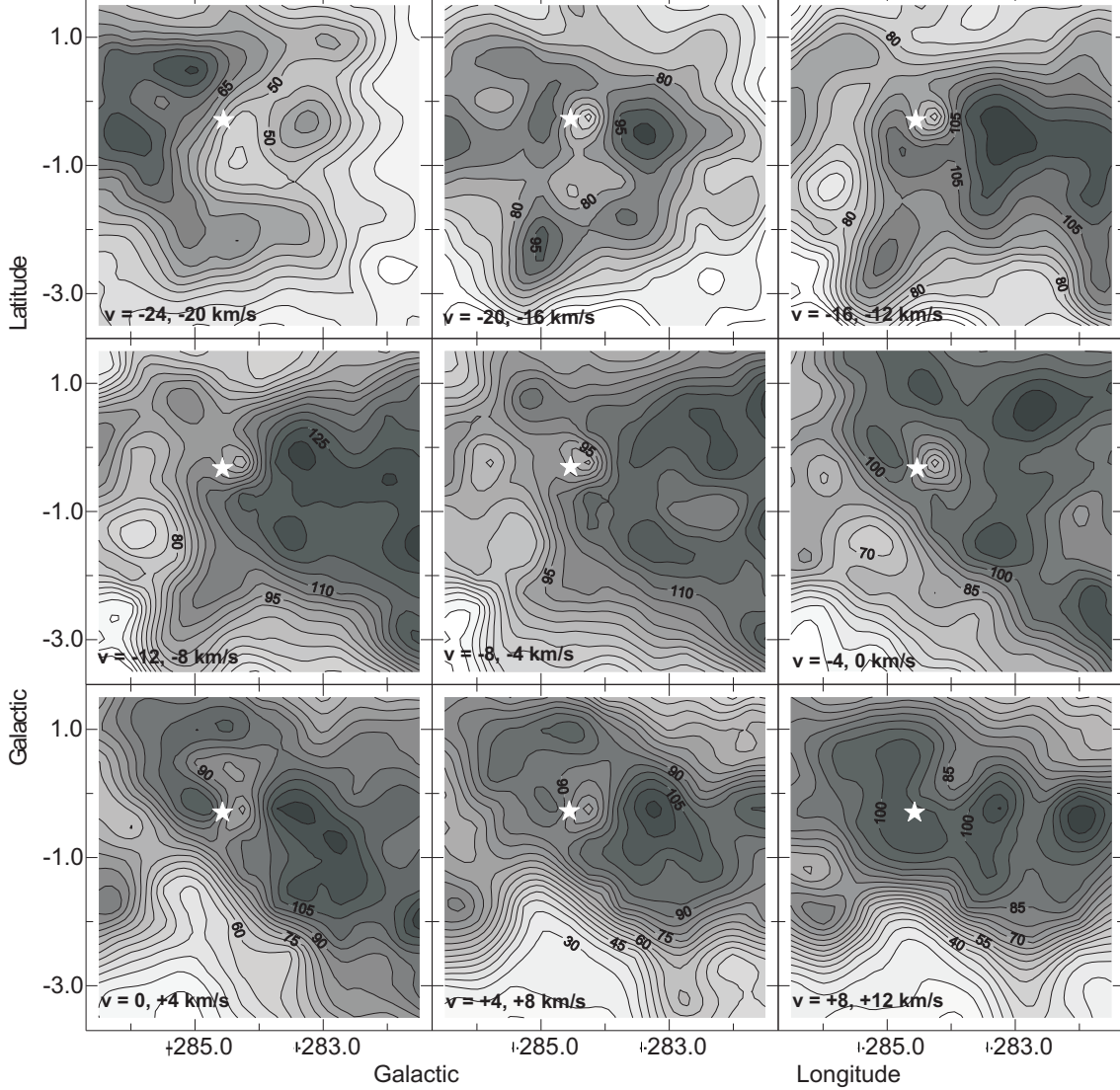


Fig. 2. H I-brightness temperature distribution of the Galactic emission as measured with the IAR telescope (HPBW = 30 arcmin) over a velocity range from -24 to $+12 \text{ km s}^{-1}$, in steps of 4 km s^{-1} . The position of WR 21a is marked with a white star. The contour levels indicate H I brightness temperatures in steps of 5 Kelvin.

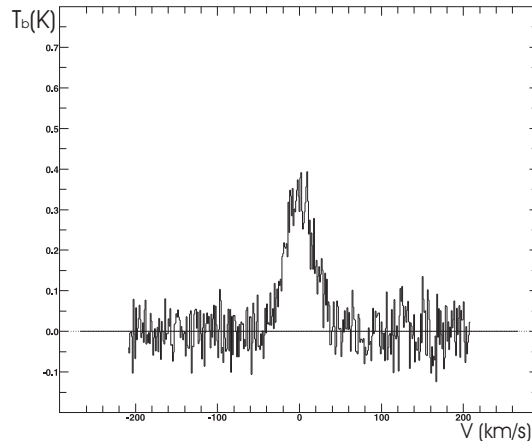


Fig. 4. 3.3 GHz radio recombination line H125α towards RCW 49. HPBW = 12.4° .

Finally, a wind mechanical energy $E_w = L_w t = 2.6 \times 10^{51}$ erg per Myr is obtained if both stars are considered, and $E_w = 1.2 \times 10^{51}$ erg per Myr for only WN6. It can be seen that the energy deposited by the wind is much larger than the energy needed to create a typical bubble.

6. The X-ray history of WR 21a

Among the Wolf-Rayet stars, WR 21a is especially prominent in X-rays: despite its modest optical magnitude, it is one of the five or six brightest sources in both apparent and absolute terms. Since the discovery of 1E 1024.0–5732 in 1979 with the *Einstein* Observatory by Goldwurm et al. (1987), through its identification with a Wolf-Rayet star by Mereghetti et al. (1994), WR 21a has been observed on ten separate occasions in X-rays as shown in Table 3. All of these data are available through the HEASARC.

As we mentioned before, Reig (1999) compared his 1997-*RXTE* data with earlier Einstein-IPC and ROSAT-PSPC measurements to show that the X-ray luminosity had apparently been steadily rising by about a factor of five in the eighteen years since its discovery and argued that this showed WR 21a is a long-period CWB of the type exemplified by WR 140 (Williams et al. 1990).

Though in general terms the latter is probably correct, the details are more complicated. First, the X-ray model which Reig used had too high an absorbing column density ($N_{\text{H}} = 2.9 \times 10^{22} \text{ cm}^{-2}$) to be consistent with the soft X-ray data; and second, the faintness of the pair of ROSAT-HRI measurements made in 1994 (Belloni & Mereghetti 1994) contradicts the apparent inexorable rise in luminosity since 1979. Since the *RXTE* observation, two archived sets of ASCA data have also become available that are useful for bridging the soft X-ray images and the hard X-ray collimator data. The first ASCA observation took place two months after Reig's *RXTE* pointing though WR 21a was not the main objective and thus appeared near the edge of the GIS field-of-view, one of the two ASCA instruments that provided imaging X-ray spectroscopy. As a consequence there are no data from the SIS, the other instrument. On the other hand, data are available from the full set of ASCA instruments from an observation performed nearly a year later at the end of 1998.

We have obtained and analysed with XSPEC v11.2 all the archived spectra and associated response matrices available from the HEASARC. Despite the obvious changes in overall luminosity, we could find no evidence of any changes in the shape of the spectrum which, within the limited energy resolution available, seems to be consistent with the relatively hot few keV thermal plasma observed from the Wolf-Rayet binaries exemplified by WR 140 (Pollock et al. 2005), in contrast with the cooler temperatures more typical of the intrinsic emission of single stars (see for example the studies on the presumably single WN stars WR 1 [Ignace et al. 2003], WR 6 [Skinner et al. 2002b], and WR 110 [Skinner et al. 2002a]). The spectrum was modeled as an absorbed Bremsstrahlung continuum with additional emission lines of Si, Mg and Ne. The best-fit values of column density and temperature were $N_{\text{H}} = 7.0 \pm 0.6 \times 10^{21} \text{ cm}^{-2}$, about a factor of 4 lower than Reig's (1999) value, and $kT = 3.3 \pm 0.2 \text{ keV}$. This empirical approach has the natural advantage of reproducing the range of ionization species in the spectrum, notably the simultaneous presence of the lines of SiXIII and SiXIV. The alternative fits given by XSPEC's plasma models were slightly worse but gave completely consistent best-fit values of column density and temperature.

The luminosities reported in Table 3 are for a joint fit to all the available spectra with only the luminosities free to vary between observations. The resulting lightcurve is shown in Figure 5. The X-ray variability is apparently irregular though the measurements are spaced at such large intervals with respect to the newly-discovered period of weeks (Niemela et al. 2005) that it will only be possible to

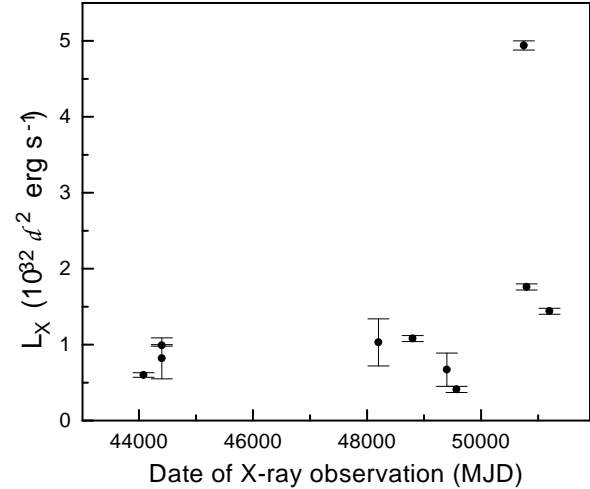


Table 3. X-ray observations of WR 21a

Date	Dataset ID	Instrument	Time (s)	Count Rate (s^{-1})	$L_X(1 - 2 \text{ keV})$ ($10^{32} d_{\text{kpc}}^2 \text{ ergs}^{-1}$)
1979-07-13	3341	Einstein-IPC	1324	0.036 ± 0.002	0.60 ± 0.03
1980-07-08	7715	Einstein-IPC	7680	0.0592 ± 0.0002	0.99 ± 0.01
1980-07-10	7716	Einstein-HRI	7006	0.006 ± 0.002	0.82 ± 0.27
1990-10-01	RS932717N00	RASS	180	0.0778 ± 0.0233	1.03 ± 0.31
1992-07-29	RP400329N00	ROSAT-PPSC	8396	0.0817 ± 0.0031	1.08 ± 0.04
1994-01-14	RH201611N00	ROSAT-HRI	696	0.0177 ± 0.0059	0.67 ± 0.22
1994-07-31	RH201611A01	ROSAT-HRI	17906	0.0108 ± 0.0012	0.41 ± 0.04
1997-11-29	301120101	RXTE-PCA	12000	7.088 ± 0.079	4.94 ± 0.06
1998-01-21	26014000	ASCA-GIS2	36858	0.0518 ± 0.0012	1.76 ± 0.04
1998-12-27	46009000	ASCA-GIS2	21174	0.0817 ± 0.0020	1.44 ± 0.04
		ASCA-SIS0	21788	0.1208 ± 0.0024	

X-rays and gamma-rays (e.g. Pollock 1987, Benaglia & Romero 2003). However, the facts that the X-ray emission from the system can be correctly modeled as thermal Bremsstrahlung and that the source has not been directly detected at gamma-rays suggest that the magnetic energy density in the CWR should largely exceed the photon energy density, implying significantly shorter cooling timescales for the synchrotron mechanism.

The same mechanism that accelerates the electrons should also operate on the ions. Synchrotron losses are not relevant for protons in the environment of the CWR. The maximum energy they can achieve will be determined by the photo-pion losses in the UV stellar field and by the size constraint imposed by the limited space available for the acceleration process. In the present case, where the CWR is not resolved and the geometry of the system remains unknown, we cannot calculate the high-energy cutoff for the non-thermal proton distribution. A value between 10 and 100 GeV seems not unreasonable (see Benaglia & Romero 2003).

It could be the case that some of these protons diffuse up to a nearby cloud where they might be trapped in the magnetic field, which is expected to be higher than the average value in the ISM (Crutcher 1999). Then they will interact there with the local material producing gamma-rays through $p + p \rightarrow p + p + \pi^0$ interactions and the subsequent $\pi^0 \rightarrow \gamma + \gamma$ decays. The situation of a passive cloud irradiated by cosmic rays from some nearby accelerator has been discussed in detail by Black & Fazio (1973) and by Aharonian & Atoyan (1996). In the present case our ignorance on several basic parameters prevents accurate calculations, but there remains the possibility that a part of the flux detected from 3EG J1027-5817 could be originated in relativistic particles accelerated in the colliding wind region of WR 21a. Whether this is or not the case could be established through future observations of the gamma-ray source by instruments like AGILE and GLAST which could report the source position with higher accuracy.

8. Summary and Conclusions

We have detected radio emission from WR 21a at 4.8 GHz. The intensity of the source is ~ 0.25 mJy. The non-detection at 8.64 GHz implies a spectral index of $\alpha < 0.3$ ($S_\nu \propto \nu^\alpha$), which significantly departs from a typical Bremsstrahlung spectrum. Combined thermal/non-thermal spectra are usually found in colliding-wind binaries. We suggest that this is also the case here, since the latest spectral determinations show that WR 21a is a system formed by WN6 and an early O companion (Reig 1999, Niemela et al. 2005). An upper limit for the system mass loss rate of $\dot{M} = 4.8 \times 10^{-5} M_\odot \text{ yr}^{-1}$ is derived from the 4.8-GHz radio flux density.

We have reanalyzed all X-ray observations of WR 21a in order to determine its time history in this waveband. Our results indicate, contrary to previous thought, that the X-ray flux has not been monotonically increasing since 1979 though the coverage is far too sparse to constrain the variability timescale. The X-ray spectrum is consistent with a few keV thermal plasma, with no obvious non-thermal contribution.

Locally accelerated relativistic electrons in the CWR probably mainly cool by synchrotron emission at radio frequencies, with small inverse-Compton losses, of which there was no X-ray evidence. If protons are also accelerated at the colliding-wind shocks, then they might diffuse through the ISM up to nearby clouds, where they might interact with an enhanced H I density to produce gamma-rays from π^0 -decays.

Future observations with both X-ray and gamma-ray instruments like CHANDRA, AGILE and GLAST can shed additional light on the nature of the high-energy emission in this interesting region. Detailed knowledge, on the other hand, of the orbital parameters of the system WR 21a will allow more sophisticated models to be built of the radiative processes taking place in the colliding-wind region.

Acknowledgements. We thank Virpi Niemela for discussions on this source. This research has been supported by the Argentine agency ANPCyT through grant PICT 03-13291.

References

- Aharonian, F.A., & Atoyan, A.M. 1996, *A&A*, 917, 928
- Bell, A.R. 1978a, *MNRAS*, 182, 147
- Bell, A.R. 1978b, *MNRAS*, 182, 443
- Belloni, T., & Mereghetti, S. 1994, *A&A*, 286, 935
- Benaglia, P., & Cappa, C.E. 1999, *A&A*, 346, 979
- Benaglia, P., Romero, G.E., Stevens, I.R., & Torres, D.F. 2001a, *A&A*, 366, 605
- Benaglia, P., Cappa, C.E., & Koribalski, B.S. 2001b, *A&A*, 372, 952
- Benaglia, P., & Romero, G.E. 2003, *A&A*, 399, 1121
- Benaglia, P., & Koribalski, B. 2004, *A&A*, 416, 171
- Bignami, G.F., & Hermsen, W. 1983, *ARA&A*, 21, 67
- Black, J.H., & Fazio, G.G. 1973, *ApJ*, 185, L7
- Brand, J., & Blitz, L. 1993, *A&A*, 275, 67
- Cappa, C.E., & Benaglia, P. 1998, *AJ*, 116, 1906
- Caraveo, P.A. 1983, *Space Sci. Rev.*, 36, 207
- Caraveo, P.A., Bignami, G.F., & Goldwurm, A. 1989, *ApJ*, 338, 338
- Cassé, M., & Paul, J.A. 1980, *ApJ*, 237, 236
- Caswell, J.L., & Haynes, R.F. 1987, *A&A*, 171, 261
- Chapman, J.M., Leitherer, C., & Koribalski, B.S., et al. 1999, *ApJ*, 518, 890
- Churchwell, E., Whitney, B.A., Babler, B.L., et al. 2004, *ApJS* 154, 322
- Crutcher, R.M. 1999, *ApJ*, 520, 706
- Dieters, S.W., Hill, K.M., & Watson, R.D. 1990, *IAU Inf. Bull.*, 3500
- Dougherty, S.M., Pittard, J.M., Kasian, L., et al. 2003, *A&A*, 409, 217
- Eichler, D., & Usov, V. 1993, *ApJ*, 402, 271
- Fich, M., Blitz, L., & Stark, A.&A, 1989, *ApJ*, 342, 272
- Grabelsky, D.A., Cohen, R.S., Bronfman, L., et al. 1987, *ApJ*, 315, 122
- Goldwurm, A., Caraveo, P.A., & Bignami, G.F. 1987, *ApJ*, 322, 349
- Goss, W.M., Radhakrishnan, V., Brooks, J.W., & Murray, J.D. 1972, *ApJS*, 24, 123
- Hamann, W.-R., Koesterke, L., & Wessolowski, U. 1995, *A&A*, 299, 151
- Hartman, R.C., Bertsch, D.L., Bloom, S.D., et al. 1999, *ApJS*, 123, 79
- Hertz, P., & Grindlay, J.E. 1984, *ApJ*, 278, 137
- Ignace, R., Oskinova, L. M., & Brown, J. C. 2003, *A&A*, 408, 353
- Koribalski, B., Johnston, S., Weisberg, J.M., & Wilson, W. 1995, *MNRAS*, 441, 752
- van der Hucht, K.A. 2001, *New Astron. Rev.*, 45, 135
- Leitherer, C., Chapman, J.M., & Koribalski, B. 1997, *ApJ*, 481, 898
- Manchester, R.N., Robinson, B.J., & Goss, W.M. 1970, *Aust. J. Phys.*, 23, 751
- McClure-Griffiths, N.M., Green, A.J., Dickey, J.M., et al. 2001, *ApJ*, 551, 394
- Mereghetti, S., Belloni, T., Shara, M. & Drissen, L. 1994, *ApJ*, 424, 943
- Moffat, A.F.J., Shara, M.M., & Potter, M. 1991, *AJ*, 102, 642
- Morras, R., & Cappa, C.E. 1995, *IAR Internal Report No. 74*
- Mücke, A. & Pohl, M. 2002, in "Interacting Winds from Massive Stars", eds. A.F.J. Moffat, & N. St-Louis, ASP Conf. Ser. 260, p. 355
- Niemela, V., et al. 2005, in preparation
- Nolan, P.L., Tompkins, W.F., Grenier, I.A., & Michelson, P.F. 2003, *ApJ*, 597, 615
- Nugis, T., & Lamers, H.J.G.L.M. 2000, *A&A*, 360, 227
- Reig, P. 1999, *A&A*, 345, 576
- Pollock, A.M.T. 1987, *A&A*, 171, 135
- Pollock, A.M.T., Corcoran, M.F., Stevens, I.R., & Williams, P.M. 2005, *ApJ*, in press
- Prinja, R.K., Barlow, M.J., & Howarth, I.D. 1990, *ApJ*, 361, 607
- Roberts, M.S.E., Romani, R.W., & Kawai, N. 2001, *ApJS*, 133, 451
- Rodgers, A.W., Campbell, C.T., & Whiteoak, J.B. 1960, *MNRAS*, 121, 103
- Romero, G.E. 2001, in "The Nature of Unidentified Galactic High-Energy Gamma-Ray Sources", eds. A. Carramiñana, O. Reimer, & D.J. Thompson, Kluwer, 267, p. 67
- Romero, G.E., Benaglia, P., & Torres, D.F. 1999, *A&A*, 348, 868
- Skinner, S. L., Zhekov, S. A., Güdel, M., & Schmutz, W. 2002a, *ApJ*, 572, 477
- Skinner, S. L., Zhekov, S. A., Güdel, M., & Schmutz, W. 2002b, *ApJ*, 579, 764
- Stevens, I.R., Blondin, J.M., & Pollock, A.M.T. 1992, *ApJ*, 386, 265
- Torres, D.F., Romero, G.E., Combi, J.A., & Benaglia, P. 2001, *A&A*, 370, 468
- Vacca, W.D., Garmany, C.D., & Schull, J.M. 1996, *ApJ*, 460, 914
- Vink, J.S., de Koter, A., & Lamers, H.J.G.L.M. 2000, *A&A*, 362, 295
- Völk, H.J., & Forman, M. 1982, *ApJ*, 253, 188
- Wackerling, L.R. 1969, *Mem. RAS*, 73, 153
- White, R.L. 1985, *ApJ*, 289, 698
- White, R.L., & Chen, W. 1992, *ApJ*, 387, L81
- Whiteoak, J.B.Z., & Uchida, K.I. 1997, *A&A*, 317, 563
- Williams, P.M., van der Hucht, K.A., Pollock, A.M.T., et al. 1990, *MNRAS*, 243, 662